

Addition of Noise by Scatter Correction Methods in PVI

J. Scott Barney[†], Ronald Harrop[‡] and M. Stella Atkins[‡]

[†] Div. of Nuclear Medicine, Vancouver General Hospital, Vancouver, B.C., Canada, V5Z 1M9

[‡] School of Computing Science, Simon Fraser University, Burnaby, B.C., Canada, V5A 1S6

Abstract

Effective scatter correction techniques are required to account for errors due to the high scatter fraction seen in positron volume imaging (PVI). To be effective, the correction techniques must be accurate and practical, but they also must not add excessively to the statistical noise in the image. We have investigated the noise added by three correction methods: a convolution/subtraction method; a method that interpolates the scatter from the events outside the object; and a dual energy window method with and without smoothing of the scatter estimate.

The methods were applied to data generated by Monte Carlo simulation to determine their effect on the variance of the corrected projections. The convolution and interpolation methods did not add significantly to the variance. The dual energy window subtraction method without smoothing increased the variance by a factor of more than twelve, but this factor was improved to 1.2 by smoothing the scatter estimate.¹

1 INTRODUCTION

A major motivation for the removal of septa in positron imaging is the improvement in the statistical characteristics of images due to the increased number of events detected for a given activity in the object. The signal to noise ratio in an image pixel is related to (the square root of) the variance in the projection pixels that contribute to its value[1]. This variance depends on the total counts, including true, scattered and random events. The increased scatter fraction associated with volume imaging thus increases the variance of the measured data relative to the number of true events, reducing the gains due to increased sensitivity. In spite of this, substantial improvements can be realized[2, 3], provided the processing methods required for volume imaging do not further increase the variance.

Some form of scatter reduction or correction is generally considered necessary if quantitatively accurate results are to be obtained from PVI. While methods to reduce

the number of scattered events in the measured data have been proposed[4], most methods correct the measured data by removing estimates of the scattered events[5, 6, 7, 8]. These correction methods can, at best, remove expected number of scattered events, leaving the variance of the corrected data unchanged from that in the total measured data. In practice, some additional noise is generally added. Testing of scatter correction methods has usually focused on their accuracy in estimating the unscattered data on average[9, 10, 11], without explicitly considering the statistical noise that they add to the final image.

2 EFFECT OF SCATTER CORRECTION

Scatter correction methods generally add statistical noise because the (possibly implicit) estimates of scatter are themselves based on measured data. We have examined the noise adding characteristics of three types of scatter correction methods that use different sets of measured values to estimate the true data, namely convolution/subtraction, interpolation from events outside the object, and dual energy window subtraction.

The convolution/subtraction method calculates an estimate of the scatter in each projection pixel based on the (weighted) counts in the neighbourhood of the pixel. The scatter is then subtracted from the measured pixel value. Since the scatter kernel for positron volume imaging has a broad, fairly flat distribution, the fractional standard deviation of the scatter estimate in each pixel is related to the counts over a large region of the 2D projection plane, and its variance is thus small compared to the variance in a single pixel.

As an example of the size of error expected, the standard deviation of the scatter estimate as a fraction of the true counts was calculated to be less than 0.008 at the centre of the field of view for each iteration, for the scatter kernel and source distribution described in the next section. The variance of the true count estimate at the centre is then $1.00007 * \text{var}[c_0]$ for one iteration (where c_0 is the total number of counts in the pixel).

The interpolation method estimates scatter in the projection by scaling a simple function to best fit all pixels outside the object boundary. Again the scatter estimate

¹This work was supported by the Natural Sciences and Engineering Research Council (grant A8020) and the Centre for Systems Science, Simon Fraser University.

is based on a relatively large region so the variance of the estimate will be small. In this method, though, the region used is smaller and contains fewer counts than that used in the convolution method. The number of pixels available is dependent on the relative sizes of the object and field of view.

The standard deviation as a fraction of the true counts for the interpolation method described in the next section was estimated to be 0.02. The resulting variance in the true count estimate is $1.0004 * \text{var}[c_0]$.

Dual energy window methods derive the corrected pixel value from the measured value and the value in the corresponding pixel of a projection collected in a second, lower energy window. The variance added by the correction method is related to the variance of a single pixel and so we can expect it to be worse than for the other methods. We will examine the method in more detail to determine the effect on variance.

2.1 Dual Energy Window Method

The dual energy method outlined here was developed by Grootoink *et al*[7]. Predetermined ratios of events in the two energy windows are used to improve the accuracy of the correction over simple scaled subtraction methods. The ratios used are $R_{sc_i} = s_i/s_i$ and $R_{unsc_i} = t_i/t_i$; where t_i and s_i are the true and scattered counts in pixel i for the photopeak window and t_{i_l} and s_{i_l} are the same for the lower energy window. The underlying assumption is that these ratios are dependent only on the position of pixel i .

The true counts in pixel i , t_i , can then be determined from the total counts in the photopeak window, c_i , and the total counts in the lower energy window, c_{i_l} , by

$$t_i = \frac{c_i R_{sc_i} - c_{i_l}}{R_{sc_i} - R_{unsc_i}} \quad (1)$$

In practice, c_i and c_{i_l} are measured quantities, and equation 1 produces an estimate of t_i with a variance dependent on the variance of the measured values. The variance of the estimate is given by

$$\text{var}[t_i] = \frac{\text{var}[c_i] R_{sc_i}^2 + \text{var}[c_{i_l}]}{(R_{sc_i} - R_{unsc_i})^2}$$

Ratios determined by Monte Carlo simulation (described in the next section) for the centre of the field of view were $R_{sc_0} = 0.60$ and $R_{unsc_0} = 0.35$ and, for the test cylinders, $c_{0_l} \approx 0.4c_0$; resulting in variance at the centre of the field of view of about $12 * \text{var}[c_0]$.

The dual energy window approach has several attractive features, including computational simplicity and intrinsic compensation for scatter from activity outside the field of view, which make it desirable to find a solution to the variance problem. Attempting to improve the noise performance of the method by smoothing the lower energy window data, however, presents additional problems.

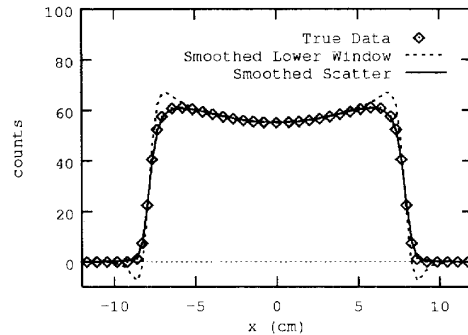


Figure 1: Noise free projection of a cylindrical flood source corrected by the dual energy window method with smoothing of the lower energy window and with smoothing of the calculated scatter component.

The lower energy window contains a significant number of unscattered events, which do not have the slow changing characteristics of scattered events. In the example above, over 65% of the events in the lower energy window pixel are unscattered. Smoothing the lower energy window data results in artifacts near edges in the image due to the blurring of these unscattered events.

In addition to the artifact problem, the variance increase remains high after smoothing the lower energy window projections. Even if the variance of the lower window data were reduced to zero, the variance would still be increased by a factor of $\left(\frac{R_{sc_i}}{R_{sc_i} - R_{unsc_i}}\right)^2$ (5.7 in the example above).

An alternative approach is to rearrange equation 1 into the form:

$$t_i = c_i - \frac{c_{i_l} R_{unsc_i} - c_{i_l}}{R_{unsc_i} - R_{sc_i}}$$

The useful feature of this form is that the fractional term corresponds to the scatter in the photopeak window, which is smoothly distributed in the projection. By isolating this component we may generate scatter projections that can be smoothed without smoothing the unscattered data. The resulting smoothed scatter values can then be subtracted pixel by pixel from the the total counts to give the estimated true counts.

The dual energy window method was applied to synthetic (noise free) projections of a cylindrical source with the lower energy window smoothed and with the scatter estimate smoothed. Figure 1 compares the true data with the projections corrected using the two approaches to smoothing. The overshoot artifact can be seen at the edge of the cylinder corrected with a smoothed lower energy window. The artifact is eliminated when the calculated scatter is smoothed instead. The noise performance of the dual energy window method without smoothing and with smoothing of the scatter estimate will be described in the following sections.

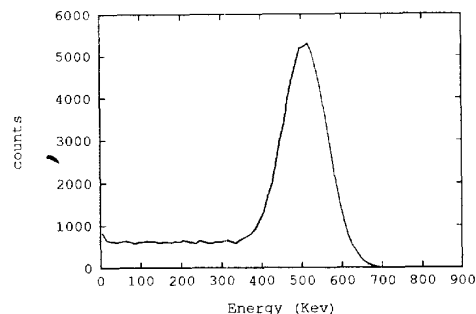


Figure 2: Energy spectrum for 511 keV gamma rays generated by Monte Carlo simulation.

3 TEST METHODS

The correction methods were tested by applying them to each of 128 projections generated by Monte Carlo simulation of a cylindrical flood source in a water cylinder. The expected number of events (scattered and unscattered) is the same for each projection because of circular symmetry, but the statistical noise in each projection is independent so the set of projections can be used as a sample from which the statistical noise properties of the corrected data can be estimated.

The scattering medium was an extended 8.5 cm radius water cylinder centred in the field of view. The source distribution was a uniform cylindrical flood with radius 8 cm, restricted to the axial field of view. The tomograph geometry approximated that of the Siemens ECAT 953B. The model of energy resolution was based on BGO block detectors, with 75% of the detected gamma rays assigned to a gaussian distributed photopeak (20% FWHM) and the remaining events distributed uniformly across lower energies. Figure 2 shows the resulting spectrum for a 511 keV gamma ray generated by Monte Carlo simulation.

Since the object of this work was to examine noise performance, the methods were tailored to the scattering object and source distribution. While this approach results in idealized correction for the expected scatter value in each case, it does not affect the statistical noise performance of the methods.

The convolution/subtraction method iteratively applied a tabulated, spatially invariant 2D kernel determined by analytic simulation[11].

The function used in the interpolation method was determined from the scatter generated by analytic simulation. The 2D interpolating function used was: $f_i = 1 + \cos(\pi r_i/25)$; where r_i is the distance (in cm) of pixel i from the centre of the field of view. To estimate scatter across the projection, this function was scaled by a factor based on the events outside the object boundary.

The dual energy method was described in the previous section. The ratios used were determined by Monte Carlo

	12M Counts		60M Counts	
	mean	variance	mean	variance
All	65.9	57.6	324.5	327.4
Unsc	52.0	51.0	255.8	256.0
Conv	51.6	57.5	253.3	327.6
Int	51.7	57.2	253.9	328.3
DEW	53.1	936.6	251.6	3981.6
S DEW	51.9	81.0	255.6	388.1

Table 1: Mean and variance for all events (All), unscattered events (Unsc) and events corrected by convolution/subtraction (Conv), interpolation (Int), dual energy window (DEW) and the dual energy window with smoothed scatter (S DEW) for a pixel in the centre of the field of view at two different total detected count levels.

simulation. In the smoothed scatter variant of the method, the scatter projections were smoothed by convolution with a 2D gaussian kernel with $\sigma = 0.625$ cm.

4 RESULTS AND DISCUSSION

The mean and variance of the central pixels of projections containing all events, unscattered events only, and events corrected each by method are shown in Table 1 for 12 million and 60 million total detected counts. Figure 3 displays the results for the 60 million count case in histogram form.

The mean value for each of the correction methods is very close to the actual mean for the unscattered projections. This is expected since the methods were set up to work well, on average, with the simulated phantom used.

The variances in the true count estimates generated by the convolution/subtraction and the interpolation methods are essentially the same as the variance in the original uncorrected data, which is as good as can be achieved. One would expect that this would extend to other, similar methods using data from relatively large regions, although convolution with an extremely peaked scatter kernel (such as an exponential function[6]) could increase the variance to some degree.

The dual energy window method increases the variance in the pixel values by a factor of twelve or more, as predicted. Rearranging the calculation to generate a scatter estimate and smoothing the scatter before subtracting from the total counts improves the factor to less than 1.2. A conservative approach was used in selection of the smoothing function and it is possible that this factor could be reduced further. The smoothing step adds extra computation to the method, but the smoothing kernel is relatively small (13×13 here) and the additional computation is not excessive.

The effect of the differences in projection pixel variance can be seen in the reconstructed images. The image cor-

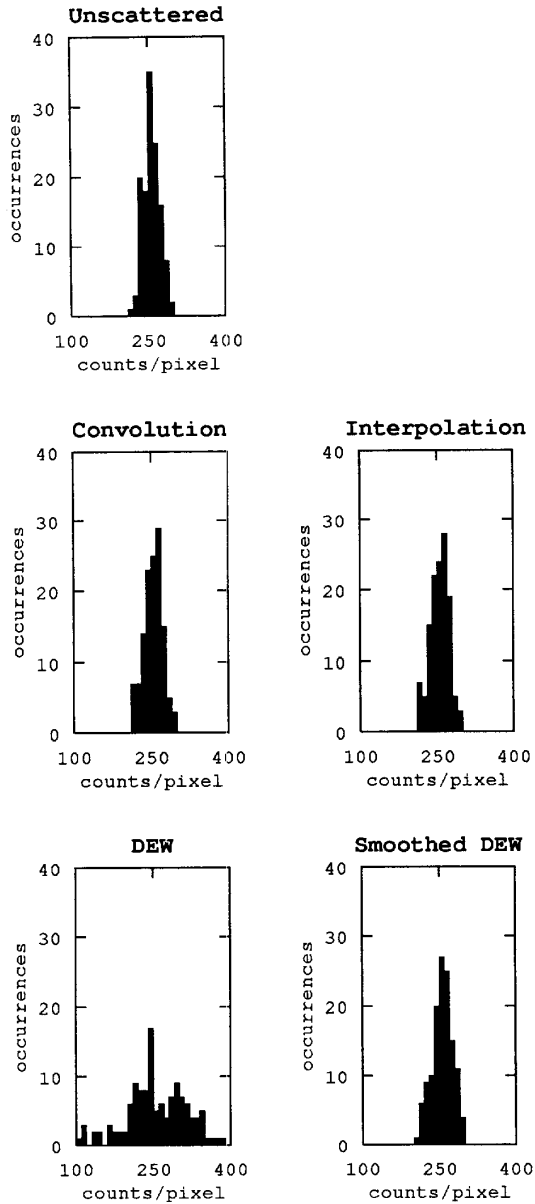


Figure 3: Histograms showing the distribution of counts in the central pixel of the unscattered projections and the projections corrected by the convolution/subtraction, interpolation and dual energy window methods and by the smoothed scatter variant of the dual energy window method.

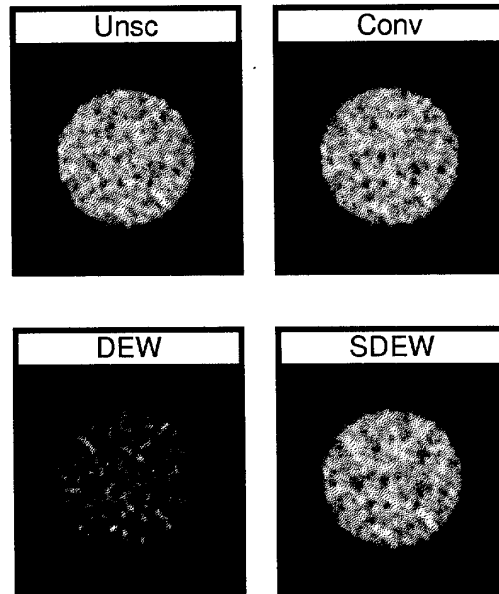


Figure 4: Images reconstructed from unscattered data only (Unsc) and from data corrected by convolution/ subtraction (Conv), dual energy window (DEW) and dual energy window with smoothed scatter (SDEW).

rected by the convolution/subtraction method is comparable to the image of the unscattered data, whereas the image corrected by the dual energy window method is considerably degraded. Smoothing the scatter estimate in the modified dual energy window method largely restores the image quality.

5 CONCLUSIONS

Although these methods have drawbacks and advantages investigated elsewhere, it is probable that each method would be useful under some set of imaging and computational requirements provided it does not add too much to the statistical noise. The convolution/subtraction and interpolation methods implemented did not measurably increase the variance in the projections, but the basic dual energy window method resulted in a large increase in variance. Smoothing the scatter estimate in the dual energy window method provided much improved noise performance without affecting the accuracy of the method.

References

- [1] S. Strother, M. Casey, and E. Hoffman, "Measuring PET scanner sensitivity: Relating countrates to image signal-to-noise ratios using noise equivalent counts," *IEEE Trans. Nucl. Sci.*, vol. NS-37, no. 2, pp. 783-788, 1990.

- [2] D. Bailey, T. Jones, T. Spinks, M.-C. Gilardi, and D. Townsend, "Noise equivalent count measurements in a Neuro-PET scanner with retractable septa," *IEEE Trans. Med. Imag.*, vol. MI-10, no. 3, pp. 256-260, 1991.
- [3] J. Barney, *Scatter Correction for Positron Volume Imaging*. PhD thesis, Simon Fraser University, 1993.
- [4] C. Thompson and Y. Picard, "Two new strategies to increase the signal to noise ratio in positron volume imaging," *IEEE Trans. Nucl. Sci.*, vol. NS-40, no. 4, pp. 956-961, 1993.
- [5] J. S. Karp, P. Kinahan, and D. Mankoff, "Positron emission tomography with a large axial acceptance angle: Signal-to-noise considerations," *IEEE Trans. Med. Imag.*, vol. MI-10, no. 3, pp. 249-260, 1991.
- [6] L. Shao and J. S. Karp, "Cross plane scattering correction - point source deconvolution in PET," *IEEE Trans. Med. Imag.*, vol. MI-10, no. 3, pp. 234-239, 1991.
- [7] S. Grootoank, T. Spinks, T. Jones, C. Michel, and A. Bol, "Correction for scatter using a dual energy window technique with a tomograph operated without septa," in *Conference Record of the 1991 IEEE Nuclear Science Symposium*, pp. 1569-1573, 1991.
- [8] J. Barney, J. Rogers, R. Harrop, and H. Hoverath, "Object shape dependent simulations for PET," *IEEE Trans. Nucl. Sci.*, vol. NS-38, no. 2, pp. 719-725, 1991.
- [9] R. L. Harrison, D. R. Haynor, and T. K. Lewellen, "Limitations of energy-based scatter correction for quantitative PET," in *Conference Record of the 1992 IEEE Nuclear Science Symposium*, pp. 862-864, 1992.
- [10] S. Grootoank, T. S. A. Kennedy, P. Bloomfield, D. Sashin, and T. Jones, "Practical implementation and accuracy of dual window scatter correction in a NeuroPET scanner with the septa retracted," in *Conference Record of the 1992 IEEE Nuclear Science Symposium*, pp. 942-944, 1992.
- [11] J. Barney, R. Harrop, and C. Dykstra, "Source distribution dependent scatter correction for PVI," *IEEE Trans. Nucl. Sci.*, vol. NS-40, no. 4, pp. 1001-1007, 1993.